PERGAMON

Neural Networks 14 (2001) 865–875

Neural Networks

www.elsevier.com/locate/neunet

2001 Special issue

Regularization mechanisms of spiking–bursting neurons

P. Varona[a,b,*], J.J. Torres[a,c], R. Huerta[a,b], H.D.I. Abarbanel[a,d], M.I. Rabinovich[a]

[a]*Institute for Nonlinear Science, UCSD, 9500 Gilman Drive, La Jolla, CA 92093-0402, USA*
[b]*GNB. Dpto. de Ingeniería Informática, ETSI, UAM, 28049 Madrid, Spain*
[c]*Dpto. de Electromagnetismo y Fisica de la Materia, Universidad de Granada, 18071 Granada, Spain*
[d]*Department of Physics and Marine Physical Laboratory, Scripps Institution of Oceanography, UCSD, La Jolla, CA 92093, USA*

Received 10 October 2000; revised 26 February 2001; accepted 26 February 2001

Abstract

An essential question raised after the observation of highly variable bursting activity in individual neurons of Central Pattern Generators (CPGs) is how an assembly of such cells can cooperatively act to produce regular signals to motor systems. It is well known that some neurons in the lobster stomatogastric ganglion have a highly irregular spiking–bursting behavior when they are synaptically isolated from any connection in the CPG. Experimental recordings show that periodic stimuli on a single neuron can regulate its firing activity. Other evidence demonstrates that specific chemical and/or electrical synapses among neurons also induce the regularization of the rhythms. In this paper we present a modeling study in which a slow subcellular dynamics, the exchange of calcium between an intracellular store and the cytoplasm, is responsible for the origin and control of the irregular spiking–bursting activity. We show this in simulations of single cells under periodic driving and in minimal networks where the cooperative activity can induce regularization. While often neglected in the description of realistic neuron models, subcellular processes with slow dynamics may play an important role in information processing and short-term memory of spiking–bursting neurons.

Keywords: Spiking–bursting neurons; Regularization; Calcium oscillations; Subcellular dynamics; CPGs

1. Introduction

There are several intracellular mechanisms that, directly or indirectly, influence the electrical activity of neurons in different time scales. Realistic models of neurons describe the dynamics of the ionic channels present in the cell membrane. Some of these channels depend on the concentration of cytoplasmic calcium ($[Ca^{2+}]$) frequently described using a first order kinetic equation. This description disregards the presence of additional subcellular processes modulating the calcium dynamics. The role that these subcellular processes play in generating different firing patterns of individual cells and circuit activity in the nervous system has not been studied in detail.

Experimental observations in crustacean CPGs show that the behavior of neurons inside the network is more regular than that of an isolated single cell (Abarbanel, Huerta, Rabinovich, Rulkov, Rowat & Selverston, 1996; Bal, Nagy & Moulins, 1988; Elson, Huerta, Abarbanel, Rabinovich & Selverston, 1999). In fact, cells such as the LP (lateral pyloric) and PD (pyloric dilator) in the stomatogastric (STG) CPG of the California spiny lobster have, when isolated from their natural connections, a highly irregular spiking–bursting activity. Nonlinear analyses of the membrane potential time series registered in these neurons show the chaotic nature of the isolated cells (Abarbanel et al., 1996). This chaotic behavior is regulated through the cooperative activity of the whole CPG in order to produce regular signals that control motor movements. The subcellular mechanisms that may be responsible for the genesis of the irregular behavior and the network interactions causing its regulation are unclear. In this paper, we present a modeling study to show how the presence of a slow dynamics (such as the calcium oscillations inside the intracellular stores) may account for the chaotic bursting activity and how different stimuli can regulate it by modulating these slow oscillations.

The realistic conductance model of the stomatogastric neurons that we use in this paper includes a detailed description of $[Ca^{2+}]$ dynamics with nonlinear calcium exchange through the endoplasmic reticulum (ER). The analysis of the time series of the spiking–bursting behavior produced by a single neuron model shows clear signs of chaotic activity similar to that observed in the experimental recordings of the stomatogastric cells. Periodically driven stimuli, such as current pulses on the isolated model neuron, can also

* Corresponding author. Tel.: +1-858-534-4068; fax: +1-858-534-7664.
E-mail address: pvarona@lyapunov.ucsd.edu (P. Varona).

0893-6080/01/$ - see front matter
PII: S0893-6080(01)00046-6

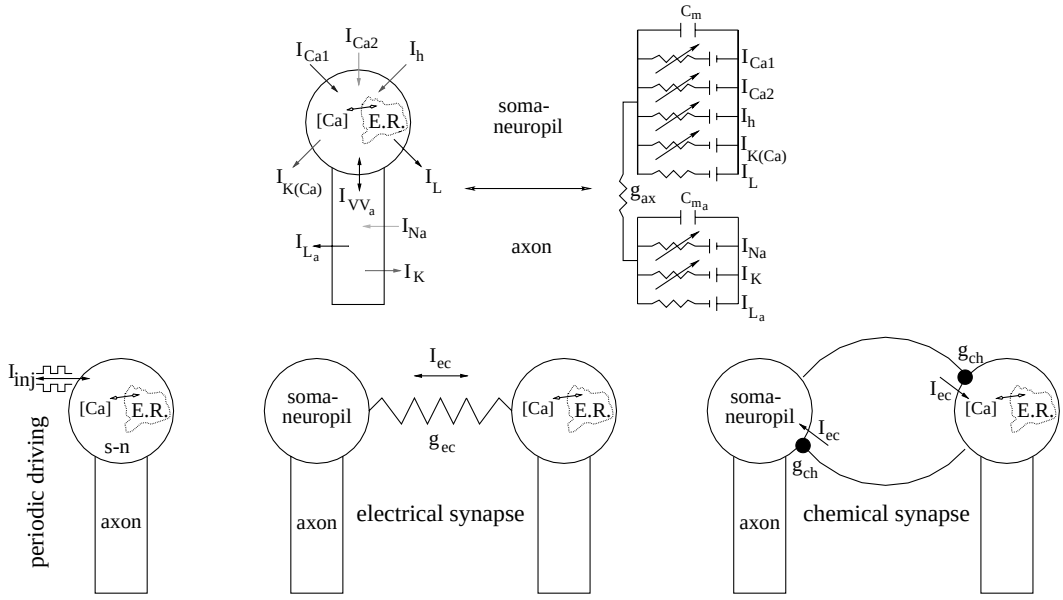

Fig. 1. Top panel: two-compartment model of a stomatogastric neuron. The model includes a detailed description of the $[Ca^{2+}]$ storage and diffusion in the endoplasmic reticulum and six active channels. Bottom panel: the three different configurations used to study the regularization phenomena: periodic driving by pulse injection for the single neuron model (left) and the minimal network simulations: two cells electrically connected at the soma compartment (middle) and the two neurons connected with mutual excitatory/inhibitory chemical synapses (right).

regulate the bursting activity, as observed experimentally. The model allows us to investigate the fundamental variables underlying this regulation of the membrane potential. We have also built a model of two coupled neurons (connected by an electrical gap junction or two mutual excitatory/inhibitory chemical synapses) to study synchronization and regularization phenomena within this minimal network. As in the single cell simulations, the slow dynamics of calcium concentration in the ER plays a major role in the regulation of the chaotic membrane potential oscillations.

Modulation of cytoplasmic and luminal calcium concentration may be part of the signaling mechanism by which intercellular connections and subcellular processing influence membrane activity. Calcium is a ubiquitous second messenger that has been implicated in a variety of events in the activity of neurons (Berridge, 1998). Our model makes interesting predictions that can be proved and extended by experimental work. The role of chaos in neural systems has been discussed widely in recent papers (Rabinovich & Abarbanel, 1998; Richardson, Imhoff, Grigg & Collins, 1998). The organization of chaotic bursting neurons in assemblies where their synchronization drives regular adaptive and reliable activity can be a general enough principle used by nature to process information and accomplish critical functionality.

2. The neuron model

We begin with a previously built model of the lobster's stomatogastric LP neuron (Falcke, Huerta, Rabinovich, Abarbanel, Elson & Selverston, 2000) that incorporates six active ionic currents distributed in two compartments (soma-neuropil and axon) depending on their slow/fast evolution (see top panel in Fig. 1). The detailed calcium dynamics for the soma compartment includes Ca^{2+} storage in the endoplasmic reticulum and Ca^{2+} transport through the luminal and through the cytoplasmic membrane. Recent studies indicate that the presence of calcium oscillations inside the endoplasmic reticulum has significant effects in the cytoplasmic membrane potential oscillations (Berridge, 1998; Li, Keizer, Stojilkovic & Rinzel, 1995a; Li, Rinzel & Stojilkovic, 1995b; Li, Stojilkovic, Keizer & Rinzel, 1997). Our simulations show that the slow calcium concentration dynamics inside the endoplasm reticulum ($[Ca^{2+}]_{er}$) may have an important role in generating and regulating the chaotic spiking–bursting activity of these neurons. The concentration of inositol 1,4,5-triphosphate (IP_3) receptor appears as a control parameter in this model. The presence of this receptor has not been reported in STG neurons but the principles of our modeling will remain the same for any other receptor regulating the calcium oscillations.

A complete description of the currents (conductance variables described by Hodgkin–Huxley and Goldman–Hodgkin–Katz formalisms) and the calcium dynamics can be found in the Appendix (see also Falcke et al., 2000, for a detailed explanation of the equations and their parameters). Although the model reproduces the main features of the spiking–bursting activity of any neuron in the pyloric STG, it was modified to yield a better description for the isolated PD neuron. This was achieved by small alterations in the kinetics (-15 mV shift), in the maximal conductances for some of the ion channels ($g_{Na} = 77\ \mu S$, $g_{Ca1} = 0.162\ \mu S$), and in the

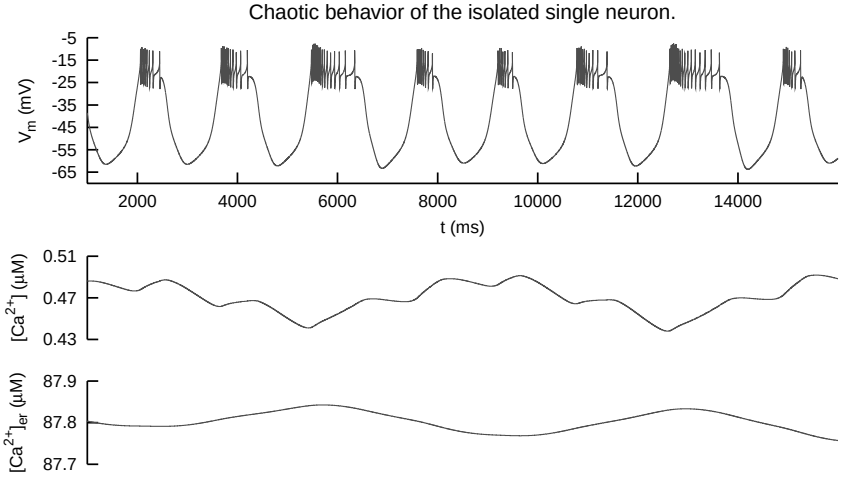

Fig. 2. Irregular spiking–bursting behavior of the isolated model neuron: from top to bottom: membrane potential V_m, cytoplasmic calcium concentration ($[Ca^{2+}]$), and calcium concentration inside the endoplasmic reticulum ($[Ca^{2+}]_{er}$).

parameters controlling the time constant for the activation of I_{Ca2}. The calculations shown in this paper use the PD model in simulations of single neurons under periodic driving, and in simulations of two coupled cells. For the network experiments we used two connectivity schemes (electrical and chemical coupling) as shown in Fig. 1 (bottom panel).

In order to have a quantitative description, the power spectrum and a measure of the entropy for its harmonics was used to evaluate the degree of irregularity in the different time series discussed in the text. The harmonic power spectra $P(n)$ were calculated using a fast Fourier transform. These were converted to probability values $p(n) = P(n)/\sum P(n)$. An entropy function (in bits), $S = -\sum p(n)\log_2[p(n)]$, was used to give a quantitative measure of the complexity of the power spectrum associated with the different time series obtained from the simulations. In this measure, a power spectrum with a single peak (a linear periodic system) yields $S = 0$ bits. A spectrum with two isolated peaks, namely, a linear quasi-periodic system with two possible states, gives $S = 1$ bit. A flat or white spectrum extending to 40 Hz yields $S = 14.35$ bits. Low values of S, relative to 14.35 bits, are then interpreted as associated with lower complexity in the oscillations of the system.

3. Results

3.1. Single neuron behavior

For all simulations described in this paper—both single neuron and two coupled neuron experiments—the model parameters were set in the regime where the isolated neuron behavior was chaotic (see Falcke et al., 2000, for a detailed characterization of the chaos in the single neuron model). Fig. 2 shows a typical time series of the spiking–bursting behavior that the single neuron model exhibits in the absence of any external stimuli. When isolated from any excitation or inhibition, the neuron fires bursts of irregular width. Membrane potential bursts range from half a second to 2 s without periodicity. The number of spikes on the top of the slow waves also changes from burst to burst; the adaptation observed in the experiments (Elson et al., 1999) is reproduced by the model.

Throughout this paper we will use three main variables to discuss the model behavior: the membrane potential V_m, the cytoplasmic calcium concentration ($[Ca^{2+}]$) and the calcium concentration inside the endoplasmic reticulum ($[Ca^{2+}]_{er}$). Note that $[Ca^{2+}]$ local maxima mark the end of V_m burst plateaus due to the effect of the hyperpolarizing $K(Ca)$ current. Luminal $[Ca^{2+}]_{er}$ evolves and slowly modulates (in anti-phase) the faster oscillations of cytoplasmic $[Ca^{2+}]$ affecting the length of the voltage plateaus. The Fourier spectrum calculated for the free-running bursting neuron, depicted later in Fig. 6a, shows a wide distribution with no sharp peaks. The entropy value calculated (as described in the previous section) for this time series was $S = 4.94$. We will use this value as a reference to discuss the regularity of the membrane potential in all simulations.

3.2. Response to periodic pulses

The result of the direct action of an ordered periodic forcing to a chaotic oscillator depends strongly on the frequency and the waveform of the signal. Both amplitude and phase are critical in determining the response of chaotic motions to external forcing. It is observed experimentally that, when isolated from phasic, chemical synaptic input, an STG neuron under periodic hyperpolarizing pulses experiences a strong, frequency-dependent regularizing action (Elson et al., 1999). Thus, regularization of chaotic bursting behavior of an isolated neuron can be obtained by injecting periodic

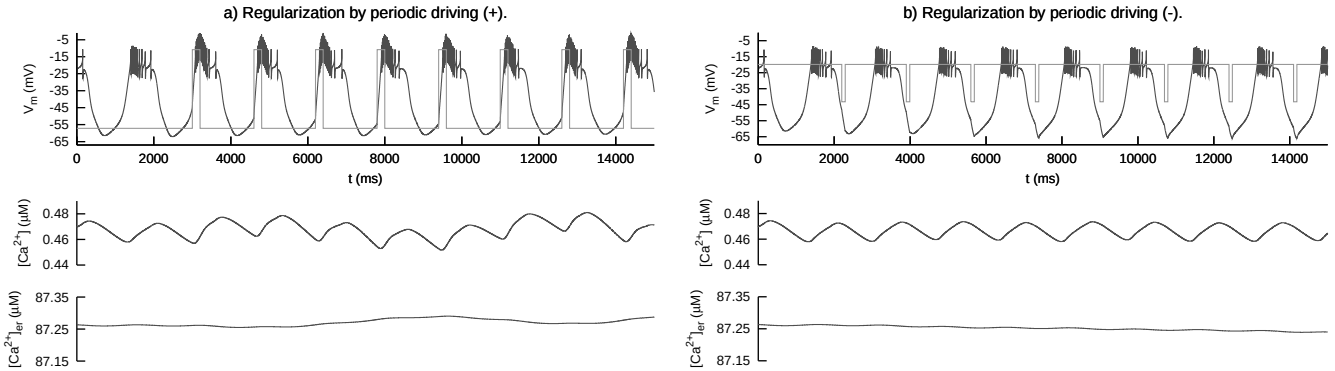

Fig. 3. (a) Burst regularization by positive current pulse injection, (b) burst regularization by negative current pulse injection. From top to bottom: membrane potential V_m, cytoplasmic calcium concentration ($[Ca^{2+}]$), and calcium concentration inside the endoplasmic reticulum ($[Ca^{2+}]_{er}$).

pulses of current to the soma. Depolarizing and hyperpolarizing pulses affect both the timing and the length of burst. Falling during the interburst phase, a depolarizing pulse can trigger a new burst; falling during an ongoing burst, it can either end the burst phase or sustain it for a little longer. Hyperpolarizing pulses (mimicking inhibitory input) strongly affect burst timing and regularize the pattern, usually driving the neuron to burst with the same frequency as the pulses.

We have reproduced these experiments using the model of the PD neuron. The model results are in good accordance with the behavior recorded in the laboratory as can be seen in Fig. 3 (cf. Fig. 2 in Elson et al., 1999). This figure shows that both positive and negative periodic pulse injection regularize the otherwise chaotic bursting behavior for the isolated neuron. For positive periodic driving (0.4 nA, 200 ms long and repeated every 1600 ms), the pulses either start a new burst or hyperpolarize the membrane if the forcing falls in the middle of a burst phase (not shown). When negative pulses are applied (-0.1 nA, 90 ms long and repeated every 1700 ms), they always end the burst phase. In most simulations, we noticed a more regular spiking behavior for the negative periodic driving. The structure, maximal power of the Fourier spectrum and the addition of local peaks at the phasic responses of the forcing signal for these two cases can be seen in Fig. 6. In both cases, sharp peaks appear in the Fourier spectrum corresponding to the driving frequency and its multiples (cf. Fig. 6b and c). The entropy values were $S = 2.27$ bits and $S = 2.63$ bits for positive and negative pulses, respectively, showing a strong regularization ($S = 4.94$ for the isolated neuron). The width of the regularized bursts depends on the driving frequency (for those frequencies in which bursting activity is sustained).

Note that in Fig. 3 the calcium concentration inside the endoplasmic reticulum remains nearly constant when the regularization is obtained by the periodic driving of the pulses. The cytosolic calcium concentration oscillates with the same frequency as the membrane potential bursts. In the following sections we will show that this is always the behavior of the slow dynamics whenever the stimulus or the cooperative behavior induces regular spiking–bursting activity.

3.3. Regularization by cooperative behavior

3.3.1. Electrical coupling

The dynamic clamp technique (Sharp, Oneil, Abbott & Marder, 1993) allows the experimenter to change the conductance of natural electrical coupling between two real neurons. Several interesting bifurcations in the dynamics of the cooperative behavior can be found using this technique. Depending on the strength and sign of the coupling between two PD neurons, different collective behaviors are observed as described in Elson, Selverston, Huerta, Rulkov and Abarbanel (1998a): from independent chaotic bursting to synchronized chaotic bursting and antiphase regular activity. Negative conductance coupling can be used between the neurons to approximate a graded inhibitory synapse. Although this kind of coupling is not present in the real CPG, it can be easily implemented in in vitro experiments using the dynamic clamp. This allows us to study a wider range of bifurcations in the cooperative dynamics of real neurons with the coupling strength as the only variable parameter. We have reproduced these four sets of experiments changing the conductance of two coupled PD model neurons with special attention to the case that induces regularization. During the simulations, a current $I_{ec1} = g_{ec}(V_{m2} - V_{m1})$ is injected into neuron 1 and the same current with negative sign is injected into neuron 2 (see Fig. 1). The strength of the electrical coupling g_{ec} is the only parameter changed in the simulations described in this section.

When the two PD model neurons are coupled with null or small coupling conductance ($g_{ec} \approx 0.01$ nS), independent chaotic behavior is observed as depicted in Fig. 4a. Membrane potential bursts range from half a second to 2 s without periodicity as in the case of an

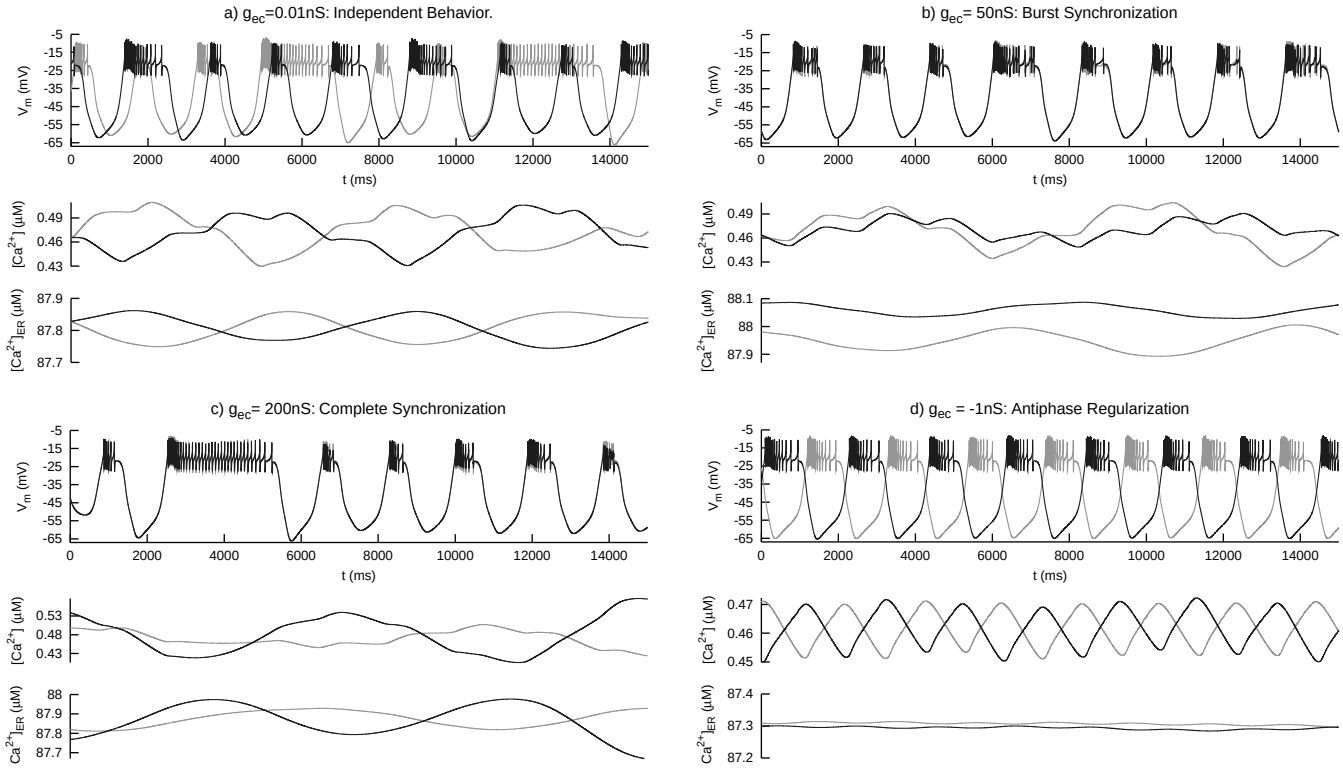

Fig. 4. Four different collective behaviors observed when two PD model neurons are coupled electrically: (a) independent chaotic bursting activity; (b) burst synchronization; (c) total synchronization and (d) anti-phase synchronization with regularization. Activity of neuron one is plotted with a dark trace; neuron two is represented with a light trace. In each of the graphs, from top to bottom: membrane potential V_m, cytoplasmic calcium concentration ($[Ca^{2+}]$), and calcium concentration inside the endoplasmic reticulum ($[Ca^{2+}]_{er}$).

isolated neuron. Calcium concentration inside the endoplasmic reticulum ($[Ca^{2+}]_{er}$) evolves slowly modulating (in anti-phase) the faster oscillations of cytoplasmic $[Ca^{2+}]$ and affecting the length of the voltage plateaus. We will discuss the evolution of these three variables for the different coupling strengths.

A moderate value ($g_{ec} \approx 0.05\ \mu S$) for the coupling conductance between the two model neurons causes burst (slow wave) synchronization, but—as a close examination shows—spike synchronization is absent (see, for example, spikes on top of bursts 4, 7, and 8 in Fig. 4b). This synchronization of the slow waves is the observed behavior for two real stomatogastric neurons interacting with their natural electrical coupling (the conductance associated with the electrical coupling between these types of neurons is ($g_{ec} \approx 0.100$–$0.200\ \mu S$ in their natural state). Note that, in our simulations for this conductivity range, $[Ca^{2+}]$ and $[Ca^{2+}]_{er}$ oscillate in a similar fashion for both neurons but they are not completely in phase, in spite of the existing burst synchronization for the membrane potential.

When the two model neurons are coupled with a high electrical conductance, $g_{ec} \approx 0.2\ \mu S$, complete synchronization both for slow waves and fast action potentials is observed (see Fig. 4c). Again, note that $[Ca^{2+}]$ and $[Ca^{2+}]_{er}$ do not oscillate in phase between the two neurons, in spite of the existing synchronization in their membrane potentials V_m caused by the high coupling conductance.

For all three cases discussed so far, small, medium and high positive coupling conductance, the bursting activity remains irregular regardless of the degree of synchronization (see Varona, Torres, Abarbanel, Rabinovich & Elson, 2001, for a detailed study and quantification of the synchronization between these two neurons). Thus, synchronization occurs without regularization. When the two neurons are coupled with a small negative conductance $g_{ec} \approx -0.001\ \mu S$, inverting the sign of the current coming from the electrical coupling in both neurons, anti-phase synchronization is observed in the membrane potentials (see Fig. 4d). Furthermore, the two neurons regulate their bursting behavior having small variance in the length of the bursts. The Fourier spectrum with a sharp peak at the frequency of the regularized bursts for this time series is shown in Fig. 6d. The calculated entropy for these membrane potentials indicates a strong regularization: $S = 1.57$ bits. As can be seen in Fig. 4d, $[Ca^{2+}]_{er}$ remains nearly constant for the two neurons, while $[Ca^{2+}]$ oscillates regularly but in anti-phase with respect

to the other neuron. Note that in the previous cases discussed in this section $[Ca^{2+}]_{er}$ oscillated slowly with a large amplitude. We again see that chaotic behavior is sustained in the single neuron model whenever $[Ca^{2+}]_{er}$ oscillations are present. For a small negative electrical coupling, the calcium dynamics in the ER of each neuron is maintained constant, since the fast oscillations of calcium in the cytoplasm are rapid enough and regular enough to have no influence on the slower calcium transfer through the endoplasmic reticulum membrane. Once the calcium concentration in the ER is kept constant, regularization of chaotic behavior occurs. The same behavior can be observed when the regularization is obtained by periodic driving through small periodic pulses of current injection and when the two neurons are coupled with mutual inhibitory chemical synapses as we will show in the next section. Small networks of PD neurons with electric coupling among nearest neighbors display the same regularization induced by the slow dynamics of $[Ca^{2+}]_{er}$, showing that this is also a robust mechanism when the neurons are coupled to more than one neighbor.

3.3.2. Chemical coupling

Mutual synaptic inhibition, a predominant type of interconnection in the intact CPG, induces regularization in the spiking–bursting behavior of stomatogastric neurons (Elson et al., 1999). We modeled mutual inhibition and mutual excitation between two neurons (see Fig. 1) using graded synapses, which are the main kind of chemical synapses present in the crustacean STG (Hartline & Graubard, 1992). The model of the synapse assumes that upon the arrival of a synapse from the input neuron, the description of the postsynaptic current in the target neuron is given by:

$$I_{\text{postsyn}} = g_{\text{ch}} s (V_{\text{rev}} - V_{\text{postsyn}}) \tag{1}$$

$$\frac{ds}{dt} = (s_\infty - s)/[\tau(1 - s_\infty)] \tag{2}$$

$$s_\infty = 1/[1 + \exp(-10 - V_{\text{presyn}})/4.54] \tag{3}$$

where g_{ch} is the maximal postsynaptic conductance, V_{rev} is the postsynaptic reversal potential and V_{presyn} is the membrane potential in the presynaptic neuron. The variable s represents the synaptic activation that follows the specified first-order kinetics, and τ is its time constant. Thus, in the model, there are three main parameters that control the effect of the postsynaptic current in the target neuron: the maximum conductance, the reversal potential and the time constant. The maximum conductance and the reversal potential control the strength of the postsynaptic current while the time constant controls the duration of each synaptic event. The onset of regular oscillations induced by chemical coupling is not as instantaneous as that observed with electrical coupling due to the presence of the characteristic time constants and the non-symmetric and delayed nature of this coupling. Thus, it is not surprising that chemical synapses, depending on these parameters, have richer effects on the cooperative behavior of the two coupled model neurons.

Synchronization and regularization phenomena by mutual synaptic excitation and inhibition, respectively, are easily achieved in the spiking–bursting activity of real stomatogastric neurons using the dynamic clamp technique to establish a controllable artificial connection also described by Eqs. (1)–(3) (Elson, Maher, Varona, Torres, Rabinovich, Abarbanel et al., 1998b; Sharp, Skinner & Marder, 1996). Our model of two PD neurons coupled with mutual synaptic excitation or inhibition reproduces this behavior (see Fig. 5). As described in the previous cases with different stimuli, regularization is obtained as long as the mutual inhibition makes the slow dynamics of the luminal calcium concentration nearly constant with no abrupt oscillations. Mutual excitation induces synchronization but no regularization (cf. Fig. 5a) while mutual inhibition can induce anti-phase bursting activity between the two neurons and regularization of the burst width (cf. Fig. 5b). The Fourier spectrum obtained for a time series in which regularization of the burst width is caused by mutual synaptic inhibition is shown in Fig. 6e. The entropy value calculated for this data, $S = 2.64$ bits, points out the degree of regularization obtained by mutual inhibition.

The joint behavior of the two neurons under mutual inhibition/excitation is much richer than that observed for the electrical coupling. The regularization depends on the strength and time constant of the chemical synapses. It is possible to obtain anti-phase behavior without regularization in mutual inhibition configurations (see Fig. 5c). In this case, the model produces nonperiodic oscillations of large amplitude in the calcium concentration of the endoplasmic reticulum.

3.4. Generality of the phenomenon and regularization in the spiking activity

Fig. 6 shows a comparison of the power spectra for the time series analyzed in the previous sections. Sharp peaks indicating the preferred frequency of the regularized rhythms can be observed for the cases in which the

Table 1
Value of the entropy for the different time series discussed in the text

Experiment	Entropy (bits)
Isolated neuron	4.94
Periodic driving (−)	2.63
Periodic driving (+)	2.27
Electrical coupling	1.57
Chemical coupling	2.64

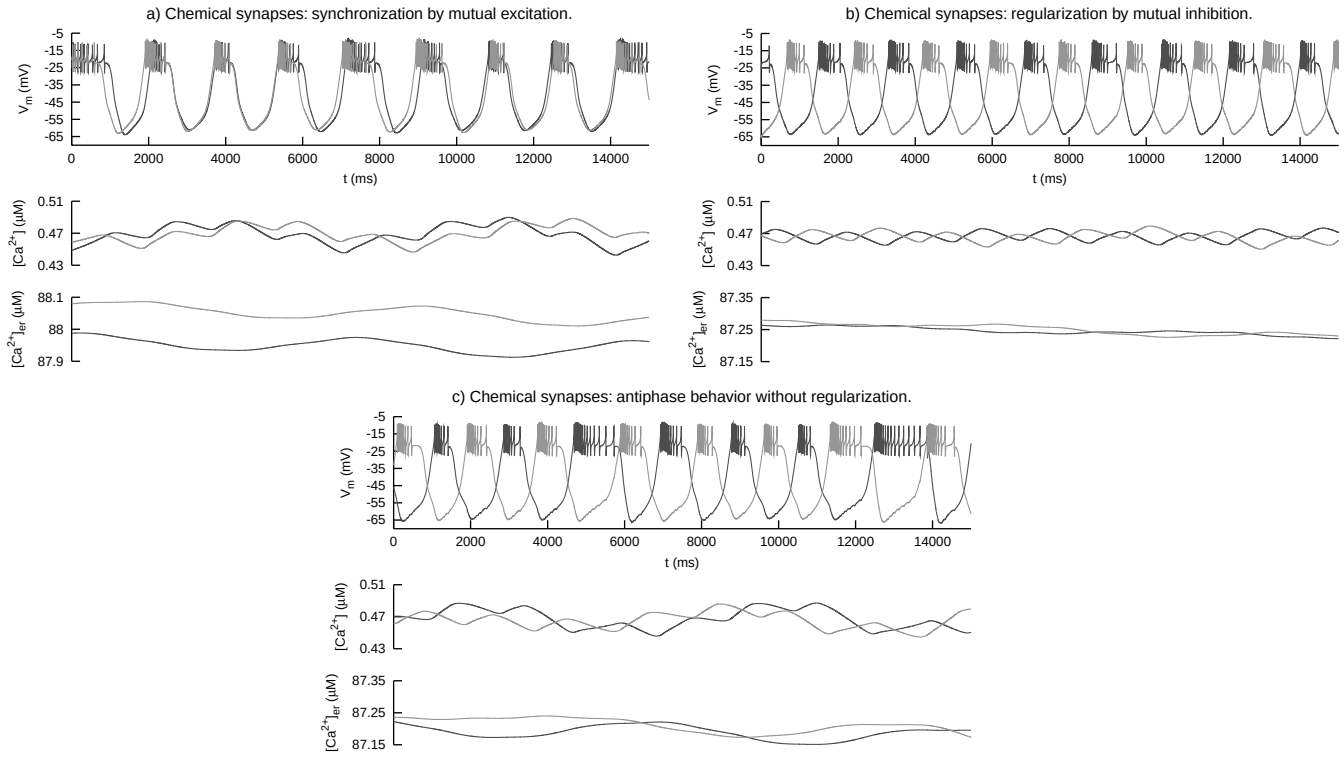

Fig. 5. Collective behaviors observed when two PD model neurons are coupled with chemical synapses: (a) synchronization by mutual excitation ($V_{rev} = 0$ mV, $\tau = 0.9$ ms, $g_{ch} = 0.1$ S); (b) anti-phase regularization ($V_{rev} = -80$ mV, $\tau = 3$ ms, $g_{ch} = 0.007$ S); (c) anti-phase behavior without regularization ($V_{rev} = -80$ mV, $\tau = 10$ ms, $g_{ch} = 0.015$ S). Activity for neuron one is plotted with a dark trace; neuron two is represented with a light trace. In each of the graphs, from top to bottom: membrane potential V_m, cytoplasmic calcium concentration (([Ca^{2+}]), and calcium concentration inside the endoplasmic reticulum ([Ca^{2+}]$_{er}$).

stimuli or the cooperative behavior yield periodic activity. Table 1 shows the values of the entropy in bits for the isolated cell and for all simulations that drive the neurons into regular behavior. Low values of S relative to the value for irregular spiking–bursting ($S = 4.94$) mean lower complexity in the oscillations reflecting the regularization.

In the model, any stimulus to a single neuron or any interaction between two neurons that induces the luminal calcium concentration to remain nearly constant causes regularization of the burst activity. The model is robust enough to reproduce all the experiments that yield periodicity in the otherwise chaotic cells.

The regularization not only affects the slow oscillation of the bursts, but also the fast spiking activity as can be seen in Fig. 7. In this figure we show the interspike interval between spike $n + 1$ and spike n in the same burst as a function of the burst number for the irregularly bursting activity of the isolated neuron (Fig. 7a), and for the regularized behavior obtained when the two neurons are electrically coupled with small negative conductances (Fig. 7b). Bottom panels in this figure show the ISI histograms for these events. Note that, as in the experimental time series (Elson et al., 1999), the beginning of the bursts has a more regular structure than its end (cf. Fig. 2). When the cooperative activity makes the burst width remain constant, the interspike intervals for the fast action potentials within the burst are also more regular.

4. Discussion

The recognition of highly irregular activity observed in the spiking–bursting activity of isolated CPG neurons raises the question of how an assembly of such neurons can cooperatively act to produce regular ordered signals to motor systems. The study of subcellular processes that affect the membrane potential activity in different time scales can contribute substantially to an understanding of how intrinsic oscillations and collective rhythms are generated. Using a realistic neuron model, we have discussed the regularization of spiking–bursting activity for single cells under periodic driving, for two neurons coupled by gap junctions, as well as for cells connected by chemical synapses in mutual inhibition. Our results indicate that a slow subcellular dynamics, here the calcium exchange

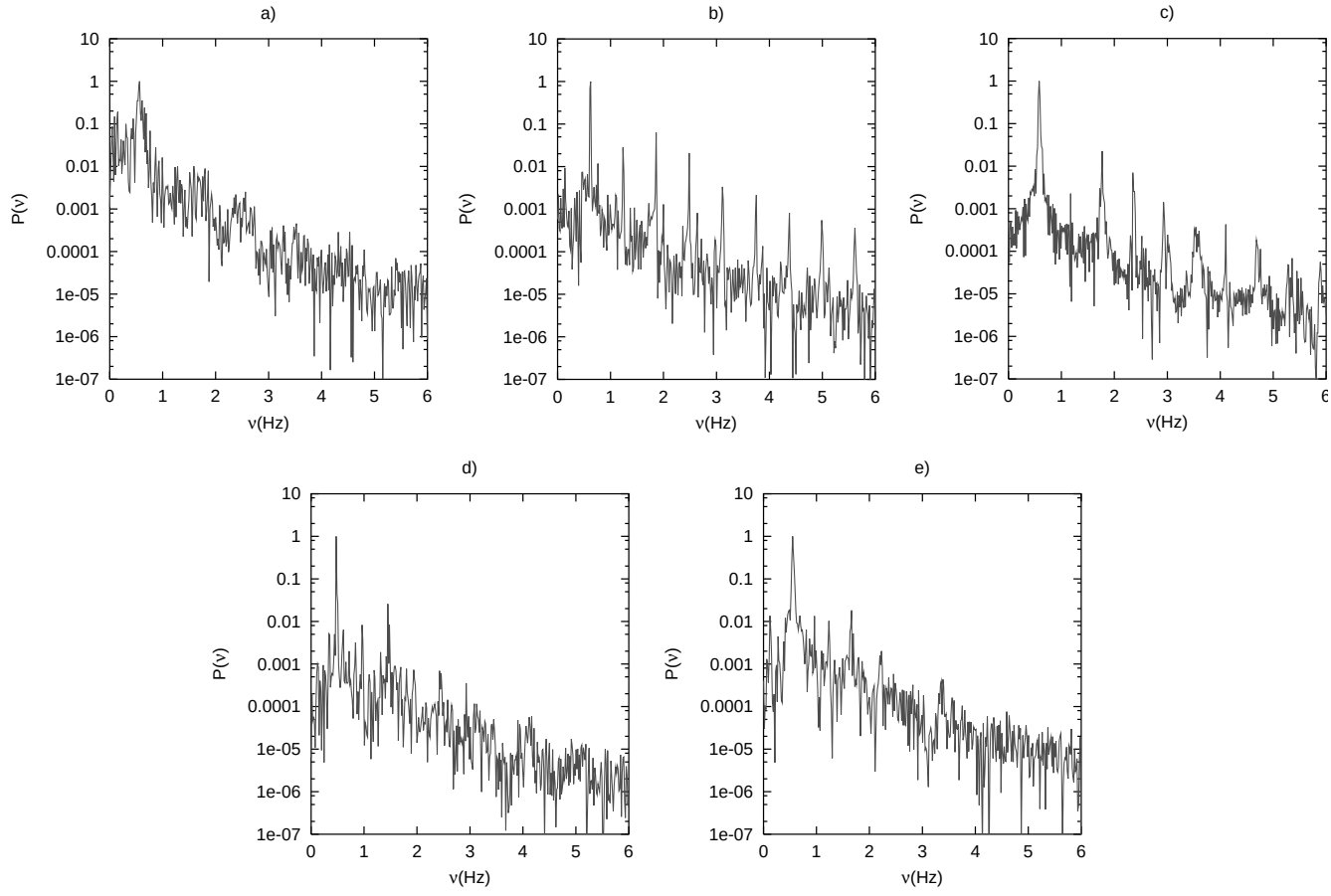

Fig. 6. Power spectra for the different time series discussed in the text: (a) isolated single neuron; (b) regularization by periodic driving (positive pulses); (c) regularization by periodic driving (negative pulses); (d) regularization by electrical coupling; (e) regularization by mutual chemical inhibition.

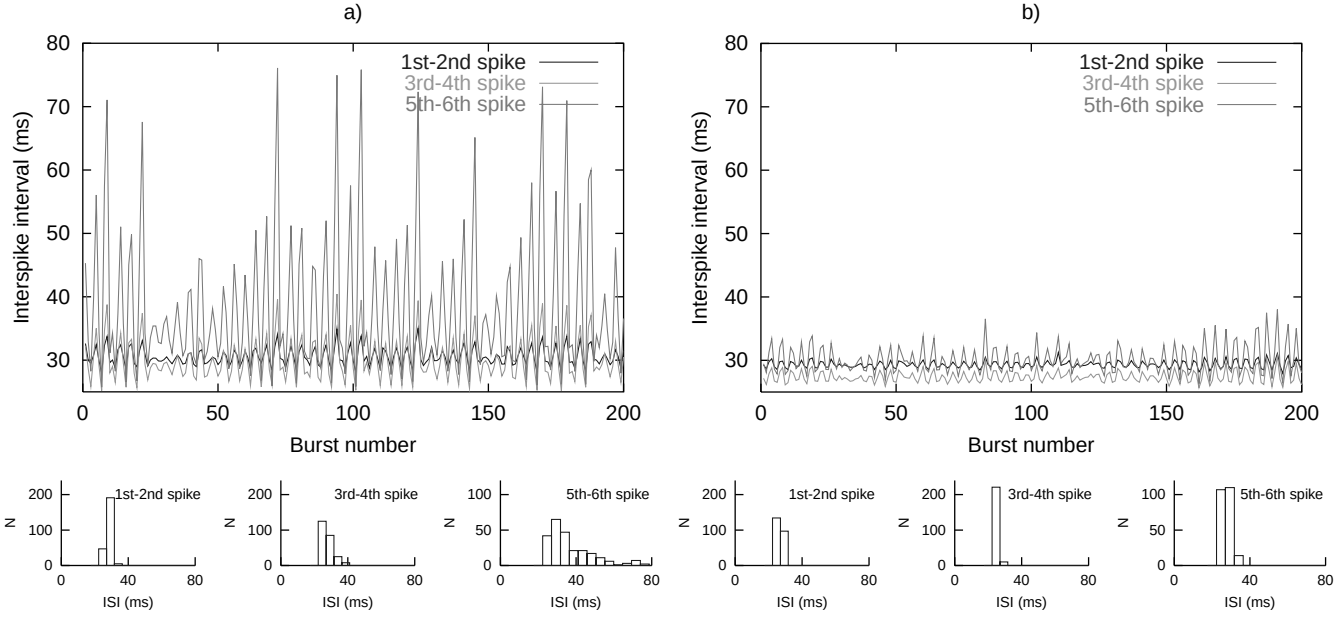

Fig. 7. Interspike interval (ISI) between spike $n + 1$ and spike n in the same burst as a function of the burst number (top panel) and ISI histograms for the same three events (bin size is 4.69 ms, calculations done over 243 bursts): (a) analysis for the isolated single neuron model; (b) analysis for the regularized behavior observed when the two neurons are electrically coupled with small negative conductance.

between the endoplasmic reticulum and the cytoplasm, can account for the origin and regularization of the chaotic spiking–bursting activity observed in the experimental recordings.

It is important to note that the same phenomenon is observed in the model when periodic stimuli are injected into a single cell or when any kind of cooperative activity between neurons induces regularization in the spiking–bursting activity: the calcium oscillations inside the intracellular store remain bounded around a steady value. The large amplitude slow modulations of the cytoplasmic calcium disappear and this makes the burst width nearly constant. In contrast, for an isolated cell or for any network topology that does not induce regularization, the oscillations of the luminal calcium modulate the calcium dynamics inside the cytoplasm causing highly irregular spiking–bursting activity.

Earlier activity is an important factor determining the actual response of a neuron. A slow subcellular process, such as the luminal calcium exchange, can act as an internal memory of the cell prior to activation. Furthermore, in networks where recurrent synapses are the predominant type of connection (i.e. CPGs), the slow dynamics can contain a short-term history of the collective rhythms and predispose the neurons to prior activity-dependent (or preferred input–output) responses.

The ability of the model to reproduce the bifurcations observed experimentally in the synchronization of two electrically coupled cells when the strength of the coupling conductance is changed confirms the robustness and flexibility of the model. Beyond reproducing in detail the features of the chaotic oscillations in stomatogastric cells, this model provides an interesting prediction about the role of subcellular dynamics in the spiking–bursting activity of neurons. This prediction, which could be tested experimentally, is supported by recent studies showing that the presence of calcium oscillations inside the endoplasmic reticulum has important effects in the cytoplasmic membrane potential oscillations (Li et al., 1995a,b, 1997).

Acknowledgements

We are most appreciative to A.I. Selverston, R.C. Elson and A. Szücs for many discussions on the model and on the experimental work reported in Elson et al. (1998a). Partial support for this work came from NSF grants NCR-9612250 and IBN-96334405. Pablo Varona and Ramón Huerta acknowledge support from MCT BFI2000-0157. Joaquín J. Torres acknowledges partial support from Universidad de Granada. Mikhail Rabinovich acknowledges support from US Department of Energy grant DE-FG03-96ER14592. Henry Abarbanel is supported in part by US Department of Energy grant DE-FG03-90ER14138 and in part by NSF grant NCR-9612250.

Appendix A. STG neuron model equations

Calcium dynamics (soma):

$$\dot{C} = j_{\text{rel}} - j_{\text{fil}} - j_{\text{out}}$$
$$\dot{C}_{\text{er}} = -(j_{\text{rel}} - j_{\text{fil}})/\sigma$$

$$\dot{h} = \frac{h_\infty - h}{\tau_h}$$

$$j_{\text{fil}} = V_{\text{erp}} \frac{C^2}{C^2 + K_{\text{erp}}^2}$$

$$j_{\text{rel}} = (P_{\text{leak}} + P_{\text{IP}_3} a_\infty b_\infty d_\infty h)(C_{\text{er}} - C)$$

$$j_{\text{out}} = v_{\text{pmp}} \frac{C^2}{C^2 + K_{\text{pmp}}^2} + v_{\text{pmex}} \frac{C^4}{C^4 + K_{\text{pmex}}^4} + \alpha(I_{\text{Ca1}} + I_{\text{Ca2}})$$

$$\Gamma(x, y, z) = \frac{1}{1 + \mathrm{e}^{(x-y)/z}}$$

$$a_\infty = \Gamma(\theta_{\text{a}} C, k_{\text{a}})$$
$$b_\infty = \Gamma(\theta_{\text{b}}, IP_3, k_{\text{b}})$$
$$d_\infty = 0.2(1 + 4\Gamma(C_{\text{er}}, \theta_{\text{d}}, k_{\text{d}}))$$
$$h_\infty = \Gamma(C, \theta_{\text{h}}, k_{\text{h}})$$

$$k_{\text{a}} = \bar{k}_{\text{a}} \left(0.8 + \frac{IP_3}{IP_3 + 0.2} \frac{0.15^2}{0.15^2 + (IP_3 - 0.4)^2}\right) \frac{60}{60 + C_{\text{er}}}$$

$$k_{\text{h}} = \bar{k}_{\text{h}} \left(0.05 + \frac{IP_3^2}{IP_3^2 + 1 + \dfrac{180}{C_{er}}}\right)$$

$$\tau_{\text{h}} = \frac{\bar{\tau}_{\text{h}}}{b_\infty d_\infty \cosh \dfrac{C - \theta_{\text{t}}}{k_{\text{t}}}}$$

Voltage dynamics (soma-neuropil):

$$\dot{V} = (-I_{\text{Ca1}} - I_{\text{Ca2}} - I_{\text{l}} - I_{\text{K(Ca)}} - I_{\text{h}} - I_{\text{V,V1}})/c_{\text{m}}$$

$$I_i = g_i m_i^{q_{i,m}} h_i^{q_{i,h}} r_i(V), \qquad \dot{n}_i = (e_{i,n} - n_i)/\tau_{i,n},$$

$$(n = m, h)$$

I_i	n	$e_{i,n}$	$q_{i,n}$	$\tau_{i,n}$	g_i	$r_i\,(V)$
I_{Ca1}	m	$\Gamma(-V-15, 33.1, 13.18)$	3	$60-40\Gamma(-V-15, 53.1, 20.5)$	0.162	$\frac{-V-15}{\exp\frac{2FV}{RT}-1.0}$
	h	$\Gamma(V+15, -23.1, 5.5)$	1	150		
I_{Ca2}	m	$\Gamma(-V-15, -4.9, 17)$	3	$37.14-25.86\Gamma(-V-15, 20.1, 26.4)$	2.76	$\frac{-V-15}{\exp\frac{2FV}{RT}-1.0}$
$I_{K(Ca)}$	m	$\Gamma(V+15, 2.5-f(C-0.5), -13)\times\Gamma(-V+15, -30.5-f(C-0.5), -3.5)\times\frac{C^4}{C^4+K^4_{K(Ca)}}$	1	5/3	0.06	$V+105$
I_h	m	$\Gamma(-V-15, -43.3, 6.5)$	1	$272+1499\Gamma(-V-15, 27.2, 8.73)$	0.024	$V+35$
I_l					0.024	$V+80$
$I_{V,V1}$					0.072	$V-V_1$

The voltage values are in mV, the g_i in μS.

Voltage dynamics (axon):

$$\dot{V}_1 = \left(-I_{Na} - I_{l1} - I_{Kd} + I_{V,V1}\right)/c_{m1}$$

$$I_i = g_i m_i^{q_{i,m}} h_i^{q_{i,h}} r_i(V), \qquad \dot{n}_i = (e_{i,n} - n_i)/\tau_{i,n},$$

$$(n = m, h)$$

I_i	n	$e_{i,n}$	$q_{i,n}$	$\tau_{i,n}$	g_i	r_i (V)
I_{Na}	m	$\Gamma(-V_1-15, 4.5, 5.29)$	3	constant: $m_{Na}=m_{Na\infty}$	77	V_1-35
	h	$\Gamma(V_1+15, -28.9, 5.18)$	1	$0.67(1.5+\Gamma(V_1+15, -14.9, 3.6))\times\Gamma(-V_1-15, 42.9, 10)$		
I_{Kd}	m	$\Gamma(-V_1-15, -7.7, 11.8)$	4	$7.2-6.4\Gamma(-V_1-15, 8.3, 19.2)$	13	V_1+105
$I_{V,V1}$					0.072	$V-V_1$
I_{l1}					0.0024	V_1+80

The voltage values are in mV, the g_i in μS.

Parameters:

$\sigma = 0.6$, $V_{cell} = 2.671$ nl, $f_{cyt} = 0.01$, $\theta_a = 0.4$ μM, $\theta_b = 0.6$ μM, $\theta_d = 20$ μM, $\theta_h = 0.36$ μM, $\theta_t = 0.35$ μM, $k_b = 0.2$ μM, $k_d = 10$ μM, $k_t = 0.18$ μM, $\bar{k}_a = 0.14$ μM, $\bar{k}_h = 0.46$ μM, $K_{K(Ca)} = 0.5$ μM, $K_{erp} = 0.2$ μM, $K_{pmp} = 0.1$ μM, $K_{pmex} = 0.9$ μM, $v_{pmp} = 0.0145$ μM s^{-1}, $v_{pmex} = 0.145$ μM s^{-1}, $P_{leak} = 0.0286\ s^{-1}$, $P_{IP_3} = 3.571\ s^{-1}$, $V_{erp} = 3.762$ μM s^{-1}, $\bar{\tau}_h = 1.2$ s, $\alpha = 0.0194$ μM $nA^{-1}\ s^{-1}$, $c_m = 0.5$ nF, $c_{m1} = 0.33$ nF, $f = 2$ V μM^{-1}, $F/RT = 0.038\ mV^{-1}$

Glossary

ER	Endoplasmic reticulum
IP_3	Inositol 1,4,5-trisphosphate
IP_3R	IP_3 receptor channel of the ER
C	cytosolic Ca^{2+} concentration
C_{er}	Ca^{2+} concentration in the ER
h	Inactivation of the IP_3R by C
$h_\infty(C)$	Equilibrium value of h
$a_\infty(C)$	Activation of the IP_3R by C
$b_\infty(IP_3)$	Activation of the IP_3R by IP_3
$d_\infty(C_{er})$	Inactivation of the IP_3R by C_{er}
j_{fil}	Ca^{2+} uptake of the ER
j_{rel}	Ca^{2+} release of the ER
j_{out}	Ca^{2+} flux across the cell membrane
θ_a	Threshold of the activation of the IP_3R by C
θ_b	Threshold of the activation of the IP_3R by IP_3
θ_d	Threshold of the inactivation of the IP_3R by C_{er}
θ_h	Threshold of the inactivation of the IP_3R by C
k_a (IP_3, C_{er})	Steepness of the dependence of a_∞ on C
$\bar{k}_a$	Parameter of k_a (IP_3, C_{er})
$k_h(IP_3, C_{er})$	Steepness of the dependence of h_∞ on C
$\bar{k}_h$	Parameter of $k_h(IP_3, C_{er})$
$k_b(IP_3, C_{er})$	Steepness of the dependence of b_∞ on $[IP_3]$
$k_d(IP_3, C_{er})$	Steepness of the dependence of d_∞ on C_{er}
$\tau_h(C)$	Time constant of h dynamics
$\bar{\tau}_h$, θ_t, k_t	Parameters of $\tau_h(C)$
σ	Ratio of the effective volume of the ER to the effective volume of the cell: $V_{er}f_{cyt}/V_{cell}f_{er}$
V_{cell}	Cell volume
V_{er}	Volume of the ER
f_{cyt}	Buffering coefficient of the cytosol
f_{er}	Buffering coefficient of the ER
V_{erp}, K_{erp}	Maximal pumping rate and half maximum value of Ca^{2+} ATPases of the ER
P_{leak}	Leak Ca^{2+} flux out of the ER
P_{IP_3}	Maximum Ca^{2+} flux out of the ER induced by IP_3 and Ca^{2+}
v_{pmp}, K_{pmp}	Maximal pumping rate and half maximum value of Ca^{2+} ATPases in the cell membrane
v_{pmex}, K_{pmex}	Maximal pumping rate and half maximum value of Ca^{2+}/Na^+ exchanger in the cell membrane
V, V_1	Soma and axon membrane voltage, respectively
c_m	Soma membrane capacitance
c_{m1}	Axon membrane capacitance
I_{Ca1}	Small maximum conductance Ca^{2+} current
I_{Ca2}	Large maximum conductance Ca^{2+} current
I_h	Low threshold current
$I_{K(Ca)}$	Ca^{2+} dependent K^+ current
I_{Na}	Fast Na^+ current
I_{Kd}	Delayed rectifier K^+ current
I_l, I_{l1}	Leak current of the soma and axon, respectively
$I_{V,V1}$	Current of ohmic coupling of V and V_1
r_i	Rectification of I_i; i is Ca1, Ca2, h, K(Ca), Na, Kd, 1, 11, or V,V1
g_i	Maximum conductance of I_i; i is Ca1, Ca2, h, K(Ca), Na, Kd, 1, 11, or V,V1
m_i	Activation variable of I_i; i is Ca1, Ca2, h, K(Ca), Na or Kd
h_i	Inactivation variable of I_i; i is Ca1 or Na
$e_{i,m}$	Equilibrium value m_i
$e_{i,h}$	Equilibrium value h_i
$\tau_{i,m}$	Time constant of m_i dynamics
$\tau_{i,h}$	Time constant of h_i dynamics
$q_{i,m}$, $q_{i,h}$	Exponent of the dependence of I_i on m_i and h_i, respectively
$K_{K(Ca)}$	Half maximum value of the C dependence of $e_{K(Ca),m}$
f	Coefficient for the shift of the threshold of $e_{K(Ca),m}$ by C
F	Faraday's constant
α	$=f_{cyt}/2FV_{cell}$

References

Abarbanel, H., Huerta, R., Rabinovich, M., Rulkov, N., Rowat, P., & Selverston, A. (1996). Synchronized action of synaptically coupled chaotic model neurons. *Neural Computation*, *8*, 1567–1602.

Bal, T., Nagy, F., & Moulins, M. (1988). The pyloric central pattern generator in crustacea: a set of conditional neuronal oscillators. *Journal of Comparative Physiology A*, *163*, 715–727.

Berridge, M. (1998). Neuronal calcium signaling. *Neuron*, *21*, 13–26.

Elson, R., Huerta, R., Abarbanel, H., Rabinovich, M., & Selverston, A. (1999). Dynamic control of irregular bursting in an identified neuron of an oscillatory circuit. *Journal of Neurophysiology*, *82*, 115–122.

Elson, R., Selverston, A., Huerta, R., Rulkov, M. R. F., Rabinovich, M., & Abarbanel, H. (1998a). Synchronous behavior of two coupled biological neurons. *Physical Review Letters*, *81* (25), 5692–5695.

Elson, R., Maher, M., Varona, P., Torres, J., Rabinovich, M., Abarbanel, H., & Selverston, A. (1998b). Regular rhythms from the mutual synaptic interaction of irregular bursters. *Society for Neuroscience Abstracts*, *24*, 154.

Falcke, M., Huerta, R., Rabinovich, M., Abarbanel, H., Elson, A. R. C., & Selverston, A. (2000). Modeling observed chaotic oscillations in bursting neurons: the role of calcium dynamics and ip3. *Biological Cybernetics*, *82* (6), 517–527.

Hartline, D., & Graubard, K. (1992). Cellular and synaptic properties in the crustacean stomatogastric nervous system. In R. M. Harris-Warrick, E. Marder, A. I. Selverston & M. Moulins, *Dynamic biological networks* (p. 77). Cambridge, MA: MIT Press.

Li, Y. -X., Keizer, J., Stojilkovic, S., & Rinzel, J. (1995a). Ca^{2+} excitability of the er membrane: an explanation for ip3-induced Ca^{2+} oscillation. *American Journal of Physiology, 269(5) Part*, *1*, C1079–C1092.

Li, Y. -X., Rinzel, J., & Stojilkovic, S. (1995b). Spontaneous electrical and calcium oscillations in unstimulated pituitary gonadotrophs. *Biophysical Journal*, *69*, 785–795.

Li, Y-X., Stojilkov, S., Keizer, J., & Rinzel, J. (1997). Sensing and refilling calcium stores in an excitable cell. *Biophysical Journal*, *72*, 1080–1091.

Rabinovich, M., & Abarbanel, J. (1998). The role of chaos in neural systems. *Neuroscience*, *87* (1), 5–14.

Richardson, K., Imhoff, T., Grigg, P., & Collins, J. (1998). Encoding chaos in neural spike trains. *Physical Review Letters*, *80* (11), 2485–2488.

Sharp, A., Oneil, M., Abbott, L., & Marder, E. (1993). The dynamic clamp—artificial conductances in biological neurons. *Trends in Neurosciences*, *16* (N10), 389–394.

Sharp, A., Skinner, F., & Marder, E. (1996). Mechanisms of oscillation in dynamic clamp constructed two-cell half-center circuits. *Journal of Neurophysiology*, *76* (2), 867–883.

Varona, P., Torres, J., Abarbanel, H., Rabinovich, M., & Elson, R. (2001). Dynamics of two electrically coupled chaotic neurons: Experimental observations and model analysis. *Biological Cybernetics*, *84* (2), 91–101.